HYDROLOGICAL PROCESSES
Hydrol. Process. **24**, 1631–1645 (2010)
Published online 11 May 2010 in Wiley InterScience
(www.interscience.wiley.com) DOI: 10.1002/hyp.7676

Comparing chloride and water isotopes as hydrological tracers in two Scottish catchments

James W. Kirchner,[1–3]* Doerthe Tetzlaff[4] and Chris Soulsby[4]

[1] *Swiss Federal Institute for Forest, Snow, and Landscape Research (WSL), CH-8903 Birmensdorf, Switzerland*
[2] *Department of Environmental Sciences, Swiss Federal Institute of Technology (ETH), CH-8092 Zürich, Switzerland*
[3] *Department of Earth and Planetary Science, University of California, Berkeley, CA 94720, USA*
[4] *School of Geosciences, University of Aberdeen, Aberdeen, Scotland AB24 3UF*

Abstract:

Time series of chloride concentrations and oxygen-18 isotopic ratios are widely used for tracing catchment storage and mixing processes and for inferring catchment travel-time distributions. However, neither chloride nor oxygen-18 is an ideal hydrologic tracer: chloride concentrations in streamwater can be affected by dry deposition, evapoconcentration and biogeochemical cycling, and water isotopes can be fractionated by evaporation. One way to test the reliability of these tracers is to determine whether, despite artifacts such as these, both tracers lead to similar inferences when measured in the same catchment. Here, we compare chloride and oxygen-18 time series in the Girnock and Allt' a Mharcaidh catchments in Scotland. Semivariograms and power spectra for both tracers exhibit similar patterns of fluctuation damping, implying that the travel-time distributions of the two tracers have similar shapes. Fluctuations of both tracers are strongly damped in streamflow compared to precipitation, implying that these catchments integrate tracer signatures over many different storm events. Streamflow fluctuations of both tracers are more strongly damped at the Allt' a Mharcaidh catchment, implying longer storage and greater mixing of waters of different ages, compared to the Girnock catchment. At both sites, streamflow fluctuations of oxygen-18 are more strongly damped, relative to precipitation, than those of chloride, leading to estimates of mean travel times that are longer, by a factor of 2–3, for oxygen-18 than for chloride. The greater variability of chloride compared to oxygen-18 may arise from spatially and temporally varying occult deposition and evapoconcentration. Nonetheless, the similarities in the behaviour of the two tracers imply that the strong tracer damping and long travel times that have been observed in many catchment studies are not artifacts, but instead reflect storage and mixing of waters over long time scales. Copyright © 2010 John Wiley & Sons, Ltd.

KEY WORDS isotopes; residence time; travel time; tracers

Received 31 August 2009; Accepted 25 February 2010

INTRODUCTION

Chloride (Cl^-) and stable isotopes of water (^{18}O and ^{2}H) have been widely used in catchment hydrology as natural tracers that are assumed to be conservative. Comparing natural fluctuations of such tracers in precipitation, soil water, groundwater and streams has provided important insights into how waters are stored and mixed, and how runoff is generated, in catchment systems. In many catchments, for example, tracer fluctuations in streams are strongly damped in comparison with those in precipitation, even during storm events. These observations imply that storm runoff is dominated by pre-event or 'old' water, which has relatively constant tracer concentrations because it averages together the tracer signatures of many previous precipitation events (e.g. Martinec *et al*., 1974; Sklash and Farvolden, 1979; Pearce *et al*., 1986; McDonnell *et al*., 1990; Neal *et al*., 1992; Buttle, 1994; Soulsby *et al*., 2000).

More recently, the simple binary notion of 'old' versus 'new' water has been superseded by the concept of a continuous distribution of travel times, representing the full spectrum of ages of waters reaching the stream. Travel-time distributions can be estimated from fluctuation time series of conservative tracers in precipitation and streamflow, using spectral analysis or time-domain convolution methods (e.g. Kirchner *et al*., 2000; McGuire and McDonnell, 2006). Inter-catchment comparisons have shown that travel-time distributions vary markedly among catchments (Hrachowitz *et al*., 2009), with inferred mean travel times being correlated with site-to-site differences in topography (McGuire *et al*., 2005), and with the relative abundance of different soil types that provide different potential for runoff generation or groundwater recharge (Soulsby *et al*., 2006; Tetzlaff *et al*., 2009). Other recent work has used long-term (i.e. 20-year) Cl^- datasets to show how fluxes of natural tracers can exhibit marked inter-annual variability as a result of climatic factors and how this may also vary transit times (Tetzlaff *et al*., 2007a; Hrachowitz *et al*., 2009).

Tracer fluctuations have also been useful in clarifying hydrological processes. Spectral analysis of daily Cl^- time series, for example, showed that catchments filter white-noise fluctuations in precipitation Cl^- inputs into fractal $1/f$ time series in streamflow (Kirchner *et al*., 2000). This fractal behaviour can be parsimoniously

* Correspondence to: James W. Kirchner, Swiss Federal Institute for Forest, Snow, and Landscape Research (WSL), CH-8903 Birmensdorf, Switzerland. E-mail: james.kirchner@wsl.ch

understood as the result of downslope advection and dispersion of spatially distributed rainfall inputs (Kirchner *et al.*, 2001), but is inconsistent with conventional tank reactor models of catchment storage and mixing. Tracer data have also provided an important constraint for hydrological models; often the streamflow hydrograph can be simulated adequately but conservative tracer fluctuations cannot, illuminating fundamental problems of model structures (e.g. Neal *et al.*, 1988). Conservative tracers are increasingly valued as 'complementary data' in the development and evaluation of hydrological models (e.g. Page *et al.*, 2007; Fenicia *et al.*, 2008).

The usefulness of conservative tracers in hydrology depends on the premise that their fluctuations reflect only the transport, storage, and mixing of water rather than other potentially confounding processes. One can question this premise in the case of both Cl^- and water isotopes. In some catchments, measured Cl^- fluxes in wet deposition are too small to account for Cl^- fluxes in streamflow, implying that dry and occult deposition are a significant fraction of the Cl^- mass balance (e.g. Page *et al.*, 2007). Evaporation can lead to significant enrichment of Cl^- concentrations in soil porewaters (Jobbagy and Jackson, 2007; Grimaldi *et al.*, 2009), and there is field and laboratory evidence that biogeochemical cycling can affect the movement of Cl^- in soils (e.g. Bastviken *et al.*, 2006; Bastviken *et al.*, 2007). Even water isotopes are not perfect tracers, because they are fractionated by evaporation (Kendall and Caldwell, 1998).

Therefore, the premise that Cl^- and water isotopes are conservative tracers in catchments is an approximation, and it is worthwhile to assess how good this approximation is. One test would be to compare the behaviour of two or more nominally 'conservative' tracers in the same catchment. Surprisingly, this has rarely been done, but for three exceptions, see Hooper and Shoemaker (1986), Neal and Rosier (1990) and Dunn and Bacon (2008).

Here, we compare Cl^- and ^{18}O time series from two Scottish catchments, to test whether the two tracers yield similar insights concerning catchment storage and mixing processes. Our analysis will focus on how much the tracers' fluctuations are damped in streamflow relative to precipitation, and on what this implies for the distribution of travel times for tracers (and thus water) moving through the catchment. If Cl^- and ^{18}O are both conservative (that is, if they both 'follow the water'), their travel-time distributions should be the same because they are carried through the catchment by the same water fluxes.

The two tracers' travel-time distributions cannot be directly measured, but their fluctuations in precipitation and streamflow can. There is a one-to-one correspondence, expressed by the Convolution Theorem (Gelhar, 1993; Bracewell, 2000), between a system's travel-time distribution and the amount that it damps fluctuations, as a function of frequency, from its input to its output. Thus, if Cl^- and ^{18}O have similar travel-time distributions, their fluctuations in streamflow should be damped by similar amounts relative to precipitation at any given frequency. We compare the damping of fluctuations in Cl^- and ^{18}O at the two sites using three approaches, at three different levels of complexity: a simple comparison of variances, a comparison of variance as a function of lag time using semivariograms, and a comparison of fluctuations as a function of frequency using Fourier power spectra. All three lines of analysis show that the degree of fluctuation damping is broadly similar between the two tracers, but different between the two study sites. These results imply that Cl^- and ^{18}O time series yield similar insights concerning catchment storage and mixing, and that both tracers are sensitive enough to detect the difference in storage timescales between our two study sites.

STUDY SITES AND METHODS

Girnock burn

The two study catchments are located in the Cairngorm Mountains of Scotland. The Girnock Burn is on the eastern side of the Cairngorms and drains a catchment of 30 km^2 (Figure 1). Average annual precipitation is 1100 mm, with annual runoff of about 700 mm (Table I). The altitude ranges from 230 m to 861 m and the mean slope is 9·9 degrees.

Higher-elevation areas are associated with granitic rocks while schists predominate at lower elevations (Soulsby *et al.*, 2007). These rocks have generally poor aquifer characteristics, and fracture flow is probably the main mechanism of bedrock groundwater movement (Robins, 1990). Much of the catchment is covered by low-permeability glacial drift deposits. Soil cover is dominated by peats and peaty gley soils on the lower catchment slopes close to the river channel. More freely draining podzols dominate the steeper upper slopes, with shallow regosols occurring at higher altitudes. Blanket bog vegetation dominates in the valley bottoms. Land use on steeper slopes is characterized by heather (*Calluna vulgaris*) moorland with small patches of forestry.

Overland flow and shallow sub-surface stormflow from the peats and gleyed soils dominate the storm hydrograph in the Girnock (Tetzlaff *et al.*, 2007b). Groundwater recharge appears to be mainly restricted to more freely draining soils (Soulsby *et al.*, 2007). Geochemically based hydrograph separations suggest that deeper groundwater sources account for *ca.* 30% of mean annual runoff (Soulsby *et al.*, 2005).

Allt a' Mharcaidh

The Allt a' Mharcaidh catchment lies on the western side of the Cairngorms. The stream drains a 10 km^2 catchment spanning an altitudinal range of 332–1111 m (Figure 1). Mean annual precipitation is 1200 mm, somewhat higher than the Girnock, and mean annual runoff is around 850 mm (Table I). Snow is also more significant at this site, and may account for up to 30% of annual precipitation (Soulsby *et al.*, 1997).

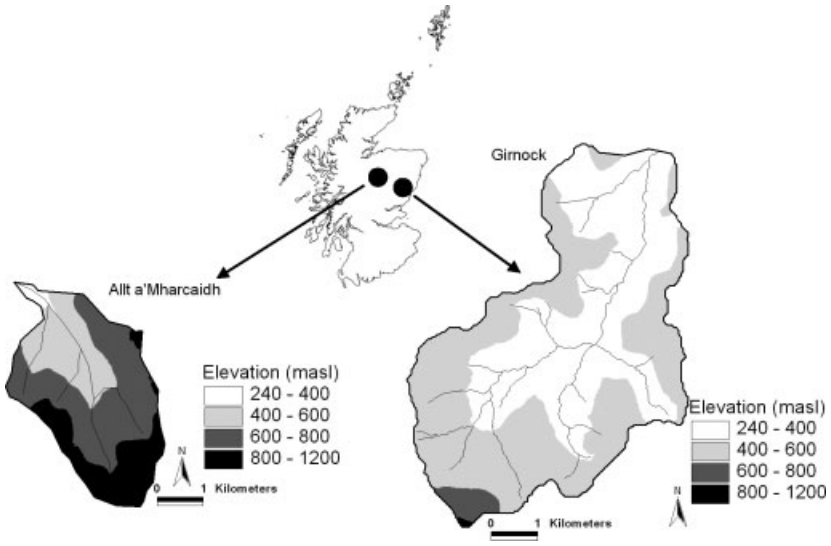

Figure 1. Location map showing the Allt a' Mharcaidh and Girnock catchments

Table I. Summary of catchment climatic, topographic and pedologic characteristics

Site		Girnock	Allt a'Mharcaidh
Area (km^2)		30	10
Annual precipitation (mm yr^{-1})		1100	1200
Annual streamflow (mm yr^{-1})		700	850
Drainage density (km km^{-2})		2·39	2·00
Median slope (degrees)		9·9	16·0
Max slope (degrees)		46	52
Mean elevation (m)		407	704
Max elevation (m)		861	1111
Min elevation (m)		230	332
HOST soil classes (% of area)	4,5,7: Alluvial soils	2	0
	15: Peaty podzols and peaty gleys	60	35
	17: Humus iron podzols	25	30
	19,22,27: Rankers	9	7
	29: Blanket peats	4	28
Geology (% of area)	Igneous—granites/diorite	54	99·8
	Metamorphic quartzite/psammite/schist	38	0·2
	Calcareous	8	0
Land cover (% of area)	Heather moorland	66	59
	Forestry	5	5
	Blanket bog/peatlands	24	0
	Montane/rocky	4	36
	Arable/improved pasture	1	0

The catchment is entirely underlain by granite which has been weathered since the Tertiary but subject to glaciation; thus the bedrock geology is covered by a range of superficial drift deposits, which, in the lower catchment, may exceed 10 m in depth and are, in places, of relatively high porosity and permeability (Soulsby *et al*., 1998). Three main soil-vegetation units occur within the catchment. At higher altitudes (c. 800 m), freely draining alpine soils have formed beneath related subarctic vegetation communities dominated by *Azalea*-lichen heath. In steeper-sloping areas up to 800 m, podzols support heather (*Calluna*) dominated boreal moorland. On gentler slopes near the valley bottom, deep peats support northern blanket bog communities dominated by *Molinia* species. The lower slopes of the catchment (below c. 450 m) support semi-natural forest dominated by Scots Pine (*Pinus sylvestris*).

Storm runoff during rainfall and snowmelt is generated mainly by saturation overland flow from the valley bottom peat soils, which may be fed by shallow sub-surface storm flow from the steeply sloping podzolic soils (Wheater *et al*., 1993; Jenkins *et al*., 1994). Vertical drainage in the freely draining alpine soils and podzols recharges groundwater in slope drifts and fractured granite (Soulsby *et al*., 1998). This in turn sustains baseflows, but may also contribute significant amounts of rapid storm runoff (Jenkins *et al*., 1994). Geochemically based hydrograph separations suggest that groundwater discharge may provide up to 50% of annual stream flows (Soulsby *et al*., 1998).

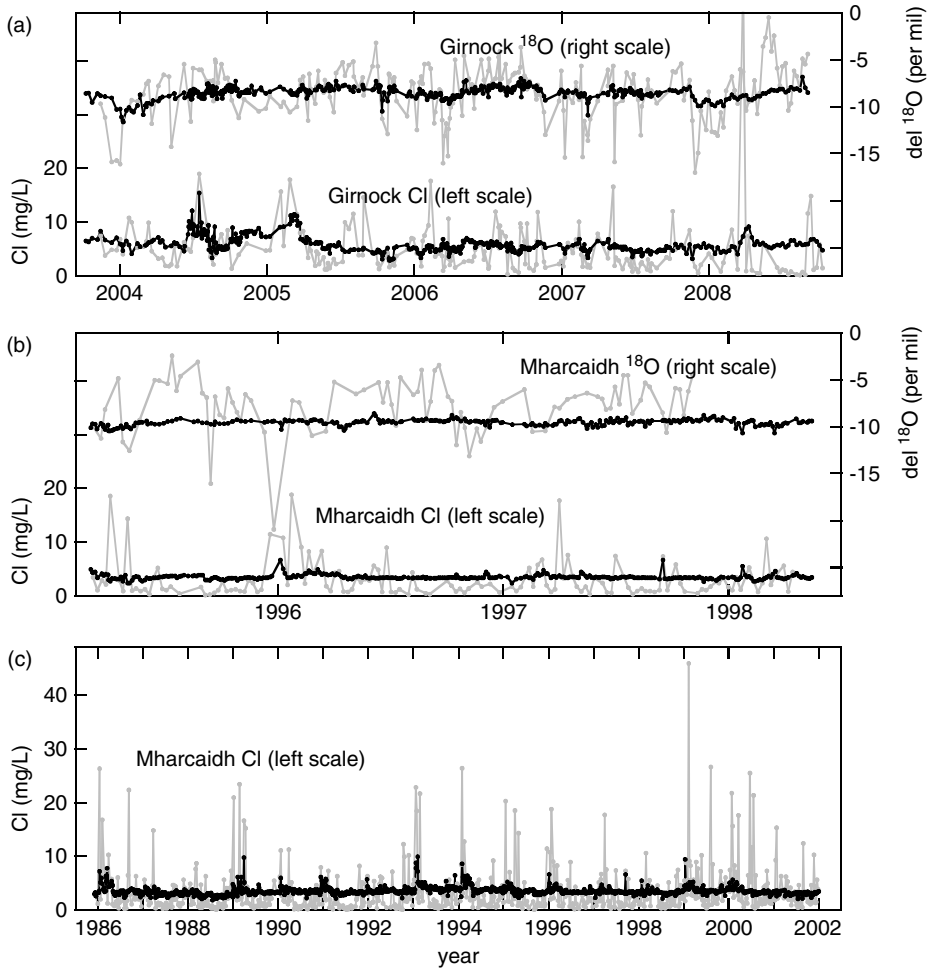

Figure 2. Time series of Cl concentrations and δ^{18}O in precipitation (grey) and streamflow (black) at the two study sites. (a) Five-year time series of Cl and δ^{18}O at the Girnock catchment. (b) Three-year time series of Cl and δ^{18}O at the Allt' a Mharcaidh catchment. (c) Sixteen-year time series of Cl at the Allt' a Mharcaidh catchment

Sampling and analysis

At both sites, plastic precipitation samplers, 20 cm in diameter, were located in the lower catchment and positioned approximately 1·5 m above ground level. These drained to underground collectors. In both catchments, accumulated bulk samples were collected at approximately weekly intervals. Automatic weather stations provided records of daily precipitation amounts.

The precipitation samplers were close to the stream gauging stations, where stream stage was recorded at 15-min intervals in natural rated sections. Instantaneous 'grab' samples of stream water were taken near the gauging stations. In the Mharcaidh catchment, samples were generally collected weekly, but in the Girnock catchment, sampling was opportunistic (whenever staff were on site) and often sub-weekly. The records from combined Cl^- and ^{18}O sampling at the Mharcaidh and Girnock catchments span approximately 3 years and 5 years, respectively (Figure 2). Records for Cl^- at the Mharcaidh catchment are available back to the mid-1980s, but because the analysis presented below seeks primarily to compare the two tracers it focuses primarily on the 3-year period that overlaps with the ^{18}O sampling.

Precipitation and streamflow samples were refrigerated after collection and analysed within 7 days. All water samples were filtered through a 0·45-μm polycarbonate membrane filter. Ion chromatography (Dionex DX100) was used to determine the Cl^- concentrations with an analytical precision of +3%. Oxygen isotope ratios were measured using a gas source isotope ratio mass spectrometer. Ratios of $^{18}O/^{16}O$ are expressed in delta units, δ^{18}O (‰, parts per mil) defined in relation to V-SMOW (Vienna standard mean ocean water). The analytical precision was approximately 0·1‰.

The use of chloride as a tracer has been questioned because of the possibility that input and output fluxes may not balance, due to potentially significant unmeasured chloride inputs as dry or 'occult' deposition. We therefore tested the chloride mass balances at our sites by multiplying the volume-weighted concentrations in precipitation and streamflow by the corresponding average water fluxes. At the Girnock catchment, the volume-weighted chloride concentrations in precipitation and streamflow are $4{\cdot}14 \pm 0{\cdot}38$ and $5{\cdot}54 \pm 0{\cdot}12$ ppm (mean ± standard error), respectively, and the precipitation and streamflow water fluxes are 1100 ± 165 and 700 ± 70 mm/year, respectively (assuming a 15% uncertainty in the annual

whole-catchment precipitation flux and a 10% uncertainty in the runoff flux). Using first-order, second-moment error propagation, we estimate the annual chloride fluxes in precipitation and streamflow, and their uncertainties, at $4{\cdot}56 \pm 0{\cdot}80$ and $3{\cdot}88 \pm 0{\cdot}40$ tonnes per square kilometer per year, respectively. Thus, the fluxes in streamflow account for 85 ± 17 percent of the fluxes in precipitation; in other words, the fluxes balance within their own uncertainties. At the Allt' a Mharcaidh catchment, the volume-weighted chloride concentrations in precipitation and streamflow are $2{\cdot}00 \pm 0{\cdot}29$ and $3{\cdot}41 \pm 0{\cdot}5$ ppm, respectively, and the precipitation and streamflow water fluxes are 1200 ± 180 and 850 ± 85 mm/year, yielding annual chloride fluxes in precipitation and streamflow of $2{\cdot}40 \pm 0{\cdot}50$ and $2{\cdot}90 \pm 0{\cdot}29$ tonnes per square kilometer per year, respectively. Thus, at the Allt' a Mharcaidh, chloride fluxes in streamflow are 121 ± 28 percent of the fluxes in precipitation; once again, in other words, the fluxes balance within their own uncertainties. These examples show that it would be risky to infer 'missing' fluxes from mass balance calculations without quantifying the associated uncertainties.

DAMPING OF TRACER VARIANCE

The tracer time series (Figure 2) show that fluctuations of both tracers are strongly damped in streamflow relative to precipitation at both sites, indicating that streamflow is averaging together waters from many previous precipitation events. It is visually apparent that fluctuations of both tracers are more strongly damped, relative to inputs, at the Mharcaidh catchment than at the Girnock, intuitively suggesting that the Mharcaidh catchment stores and mixes rainfall inputs over somewhat longer timescales than the Girnock does. It appears that within each catchment, streamflow fluctuations for the two tracers are about equally damped relative to precipitation inputs, although the damping is strong enough that the variability in the streamflow concentrations is difficult to visually assess.

The broadly similar damping in the two tracers does not arise because of any correlation between them. The variations in Cl^- and ^{18}O in precipitation are driven by different atmospheric processes, with the result that they are essentially uncorrelated with one another: the adjusted r^2 of the relationship between Cl^- and ^{18}O concentrations in precipitation is 0·03 or less at both sites, and correlations between Cl^- and ^{18}O in streamflow are even weaker. Thus, the two tracers provide independent evidence for the storage and mixing process at work in the study catchments.

One can visualize the degree of damping of the two tracers using density traces (Figure 3). Density traces are continuous functions that, like histograms (their discrete counterparts), display the local density of measured data across a range of values. They are

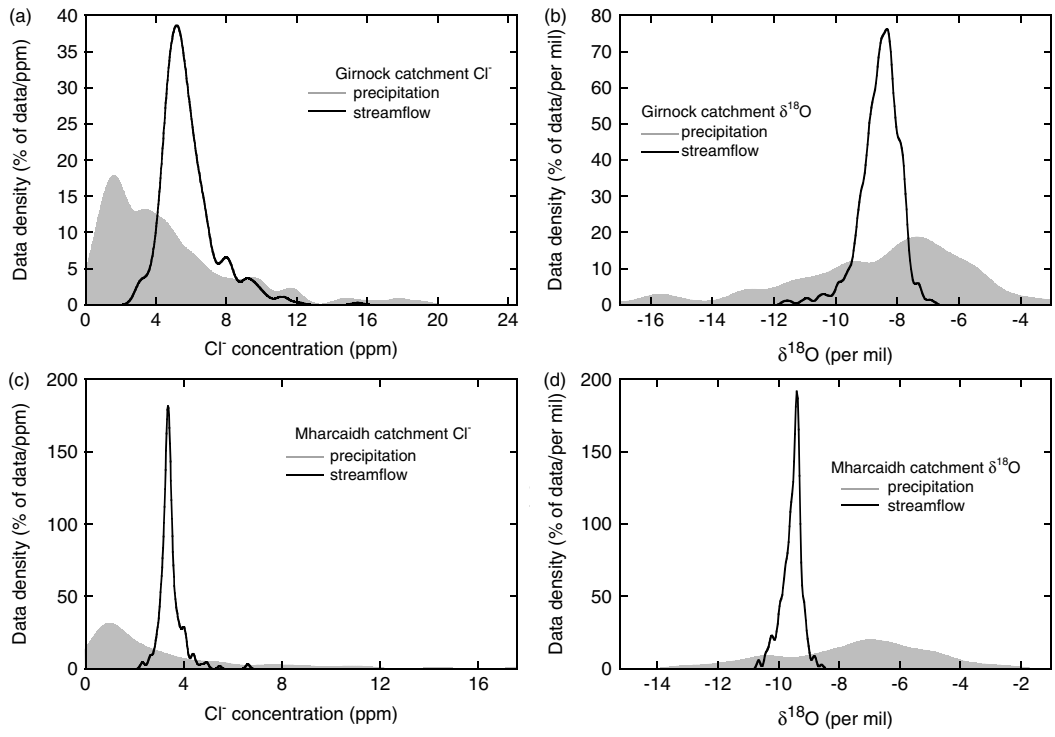

Figure 3. Density traces showing frequency distributions of Cl^- and $\delta^{18}O$ in precipitation and streamflow at the two study sites. Data density was computed by scanning a Gaussian weighting window across the range of measured values. The width (σ) of the weighting window is 1/6 of the standard deviation of the measurements, with the result that small-scale fluctuations in data density are smoothed out but the overall widths of the distributions (as measured, for example, by their standard deviations or their widths at half maximum) are not significantly altered. To make the relative degree of damping visually comparable between sites and between tracers, the horizontal axis of each plot has been adjusted to span a range equal to five times the standard deviation of the tracer concentrations in precipitation. Thus, narrower streamflow density traces correspond to tracers that are more strongly damped relative to precipitation

Table II. Damping of variance in Cl^- and ^{18}O tracers

Site	Tracer	Precipitation variance	Streamflow variance	Damping ratio (precip/stream)	Relative damping ($^{18}O/Cl^-$)
Un-weighted variances					
Girnock	Cl^- (ppm)	24·08	2·45	9·84	
Girnock	$\delta^{18}O$ (‰)	7·87	0·40	19·45	1·98
Mharcaidh	Cl^- (ppm)	12·36	0·23	53·66	
Mharcaidh	$\delta^{18}O$ (‰)	8·12	0·11	75·88	1·41
Volume-weighted variances					
Girnock	Cl^- (ppm)	11·06	2·70	4·10	
Girnock	$\delta^{18}O$ (‰)	6·24	0·76	8·21	2·00
Mharcaidh	Cl^- (ppm)	5·38	0·36	14·98	
Mharcaidh	$\delta^{18}O$ (‰)	3·86	0·15	25·71	1·72
Robust (5% trimmed) variances					
Girnock	Cl^- (ppm)	11·59	1·85	6·26	
Girnock	$\delta^{18}O$ (‰)	4·44	0·20	22·55	3·60
Mharcaidh	Cl^- (ppm)	7·43	0·11	65·53	
Mharcaidh	$\delta^{18}O$ (‰)	6·34	0·10	65·67	1·00
Semivariance of first differences					
Girnock	Cl^- (ppm)	21·79	0·48	45·76	
Girnock	$\delta^{18}O$ (‰)	3·90	0·10	39·64	0·87
Mharcaidh	Cl^- (ppm)	11·10	0·12	94·86	
Mharcaidh	$\delta^{18}O$ (‰)	5·85	0·044	133·73	1·41

an approximation to the probability density function underlying the sampled data, and like the probability density function, they are normalized so that the area under the curve is constant. Thus, narrower traces are also taller, reflecting the fact that if the distribution of the measured values is narrower, then the density of the measurements (per unit of measured value) is higher. Each panel in Figure 3 has been scaled so that the x-axis spans a range equal to five times the standard deviation in the precipitation measurements; thus, tracers that are more strongly damped will have narrower streamflow density traces.

As Figure 3 shows, both tracers at both sites have markedly narrower distributions in streamflow than in precipitation. Both tracers are visibly more strongly damped at the Mharcaidh catchment than at the Girnock, consistent with the visual impression from the raw time series shown in Figure 2. At both catchments, neither tracer appears to be much more strongly damped than the other.

One can roughly quantify the damping of fluctuations by comparing the variance of tracer concentrations in precipitation and streamflow (Table II). Table II generally confirms the visual impressions gained from Figures 2 and 3, namely, that both tracers are strongly damped at the Girnock catchment, and even more strongly damped at the Mharcaidh. Table II also indicates a general tendency for ^{18}O to be somewhat more strongly damped than Cl^- at each site.

Table II shows results from four different variance calculations, each offering a different perspective but all yielding broadly similar results for our data. The first is a conventional estimate of variance, indicating that the variance of streamflow concentrations is smaller than that of precipitation concentrations by a factor of roughly 10–20 at the Girnock catchment, and a factor of roughly 50–75 at the Mharcaidh. Variance is the square of standard deviation, so these variance ratios correspond roughly to damping of standard deviations by a factor of 3–4·5 at the Girnock catchment and 7–8·5 at the Mharcaidh. Variances in Cl^- and $\delta^{18}O$ cannot be directly compared, because they are measured in different units (ppm^2 and per mil^2, respectively), but one can compare the relative degree of damping for the two tracers by taking the ratio of the variance ratios themselves: $[Var(^{18}O_{precip})/Var(^{18}O_{stream})] \div [Var(Cl^-_{precip})/Var(Cl^-_{stream})]$. This ratio, shown in the last column of Table II, indicates that ^{18}O is damped approximately 1·4–2 times as much in streamflow, relative to precipitation, as Cl^- is. Again, these figures are in terms of damping of variance; for damping of standard deviations the corresponding figures would be approximately 1·2–1·4, the square roots of the figures given in Table II.

The interpretation of these variances would depend on whether most of the variance in concentrations arises from samples corresponding to small or large volumes of precipitation and streamflow. If, for example, the highest and lowest concentrations in precipitation are associated with trivial volumes of water, the measured precipitation variance (and thus the apparent degree of damping) will be misleadingly large. We calculated volume-weighted variances in Table II to address this possibility. The volume-weighted variances in precipitation are somewhat smaller than the conventional un-weighted variances, suggesting that concentrations associated with larger water volumes are somewhat less variable than the norm. In streamflow this pattern is slightly reversed, with volume-weighted variances slightly larger than unweighted variances, indicating that concentrations at

higher flows are somewhat more variable than the norm. The net result is that the degree of damping is smaller by a factor of roughly 2·4–3·6 when measured by volume-weighted variances rather than un-weighted variances. The relative degree of damping for ^{18}O compared to Cl^- is not greatly affected by volume-weighting of the variances, however.

Variance estimates are vulnerable to outliers. Because they are calculated as the average of squared deviations from the mean, they are particularly sensitive to the extremes of the measured values. For this reason, we also calculated the 5% trimmed variance (that is, the variance of the data after the highest and lowest 5% of the values were removed) as a variance measure that is more robust against outliers. We normalized these variances by dividing by 0·623, the 5% trimmed variance of a standard normal distribution, such that normally distributed measurements would not be affected by the trimming. The trimmed variances are generally smaller than the conventional variances, indicating that the distributions have either outliers or long tails. The damping ratios (which are not affected by the normalization described above) are broadly similar to those observed in the unweighted and volume-weighted variances, suggesting that the strong damping from precipitation to streamflow, and the stronger damping at the Mharcaidh catchment than the Girnock, are not artifacts of outliers in the data.

Finally, it is worth considering that the overall variance in a time series reflects variability on all time scales, from long-term trends to the variability between adjacent measurements. To isolate the short-term variability in the data, and to filter out the effects of seasonal patterns and long-term drift, for each of the time series we also calculated the lag-1 semivariance, the variance between adjacent data points:

$$\gamma_1 = \frac{1}{2}\frac{1}{n-1}\sum_{i=1}^{n-1}(x_{i+1} - x_i)^2 \qquad (1)$$

The leading factor of 1/2 in Equation (1)—and thus the term *semi*variance—comes from the fact that if x_{i+1} and x_i are uncorrelated, the variance of the difference between them will be twice the variance of the x values themselves. Thus, the lag-1 semivariance expresses the short-term variability of the time series in terms of the equivalent variance of a white-noise process (i.e. one that lacks any long-term correlations).

The lag-1 semivariances shown in Table II are somewhat smaller than the overall variances, indicating that some of the measured variance arises from correlations at longer lags. This effect is stronger in the streamflow time series than the precipitation time series, indicating the stronger role that longer-term correlations play in the stream data than the precipitation data. As a result, the semivariances lead to damping ratios that are greater, by roughly a factor of 2, than the others reported in Table II.

The semivariance damping ratios in Table II can be interpreted directly, albeit roughly, in terms of mean travel times for the two catchments. The Central Limit Theorem implies that if n uncorrelated quantities are averaged together, the variance of the average will be $1/n$ times the variance of the quantities being averaged. Thus, the ratio between the variance of the precipitation concentrations (the quantities being averaged) and the variance of the streamflow concentrations (the averages that result) should be approximately equal to the effective number of precipitation samples that are being averaged to determine the streamflow composition. The semivariance estimates are arguably the most reliable for estimating the variance ratio, because they measure the short-term variance in the time series without the effects of long-term correlations, which would make the Central Limit Theorem inapplicable. The median interval between precipitation measurements is 1 week, so the damping ratios for semivariances reported in Table II suggest that a typical streamflow sample at the Girnock catchment is averaging together roughly 40 weeks of precipitation, and a typical streamflow sample at the Mharcaidh catchment is averaging together roughly 95–130 weeks of precipitation. These results are broadly consistent with previously published estimates of mean travel times for these two catchments (Soulsby *et al.*, 2006; Tetzlaff *et al.*, 2007b; Hrachowitz *et al.*, 2009).

SEMIVARIOGRAM ANALYSIS

We can extend the concept of the lag-1 semivariance, developed above, to the semivariogram, which graphs the semivariance as a function of lag time. Semivariograms are widely used in geostatistics to measure variability across a range of scales (Webster and Oliver, 2007). Precipitation and streamflow were sampled irregularly at both of our sites, so finding the semivariance at a specified lag time is not as simple as solving Equation (1) for all pairs of measurements that are one, two, three, etc. samples apart. Instead, the approach we take is as follows. We take all possible pairs of points (x_i,x_j) for all i and $j \geq i$ in the time series, for a total of $n(n+1)/2$ pairs. We calculate the lag time $\tau_{ij} = t_j - t_i$ for each point pair, and sort these in ascending order. We then take groups of n pairs, starting with the n pairs with the shortest lags (which will all be lags of zero because they will be the pairs for which $i = j$), then the n pairs with the next shortest lags, and so forth. For each group of point pairs, we estimate the semivariance as:

$$svg = \frac{1}{2}\left[\langle (x_j - x_i)^2\rangle - \langle x_j - x_i\rangle^2\right], \qquad (2)$$

where the angled brackets indicate averages over all pairs i, j in the group. The second term in Equation (2) corrects for secular trends in the dataset, which could otherwise inflate estimates of the semivariance at long lags. The semivariance as defined in Equation (2) measures the variance of $(x_j - x_i)$ around its own mean, rather than around a mean of zero. The semivariance of each group of points is then plotted as a function of the average, $<\tau_{ij}>$, of the lag times for the point pairs in the group.

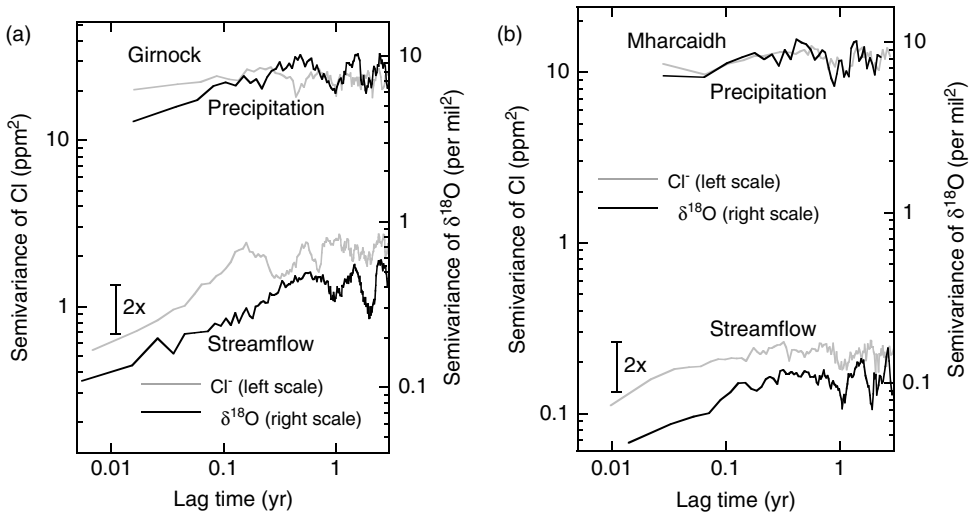

Figure 4. Semivariograms of fluctuations in Cl^- and $\delta^{18}O$ (grey and black lines, respectively) in precipitation and streamflow at the Girnock and Mharcaidh catchments. The distance between the upper and lower lines indicates how greatly fluctuations in precipitation are damped in streamflow. Each vertical axis spans the same number of log units; thus, the same vertical distance corresponds to the same damping ratio for either tracer at either site. For clarity, the axes have been adjusted so that the precipitation semivariograms for both tracers at both sites plot at approximately the same level. Therefore, the differences in damping between tracers and between sites can be estimated from the relative positions of the streamflow semivariograms. Across the full range of lag times, $\delta^{18}O$ is more strongly damped than Cl^- at both sites, and both tracers are more strongly damped at the Mharcaidh catchment than at the Girnock

Figure 4 shows semivariograms for both tracers at both sites. Figure 4 is plotted on log–log axes so that the relatively small variance in streamflow is visible on the same scale as the much larger variance of the precipitation inputs, and so that the two tracers can be directly compared despite their different measurement units. On these logarithmic scales, the vertical distance between the lines representing precipitation and streamflow corresponds to the damping ratio at any given lag time. All of the vertical scales span the same number of log units to facilitate direct comparisons. The scales have been adjusted so that the precipitation semivariograms for both tracers at both sites plot at approximately the same level. As a result, differences in damping between tracers or between sites can be directly inferred from the relative levels of the streamflow semivariograms.

The pattern of damping as a function of scale is broadly similar for both tracers at both sites. In all cases, streamflow tracer variations at shorter lag times are more strongly damped, as one would expect from mixing processes. However, even at the longest time scales shown in Figure 4 (i.e. 3 years), streamflow concentrations are at least an order of magnitude less variable, for both tracers at both sites, than the corresponding precipitation concentrations. Across the full range of lag times, both tracers are more strongly damped at the Mharcaidh catchment than at the Girnock. Also across the full range of lag times, ^{18}O is about a factor of 1·5–2 more strongly damped than Cl^- at both sites. Figure 4 is thus consistent with the results shown in Table II and Figures 2 and 3, but adds the important point that these patterns persist across a wide range of time scales, from several days to several years.

The semivariogram analyses shown above, as well as the spectral analyses presented below, are classically defined for statistically stationary systems, in which the variances of the measured signals are constant over time. By contrast, one should expect typical catchments to be non-stationary because their tracer concentrations will vary more rapidly during higher flows, and more slowly during lower flows. Even in such cases, however, a semivariogram or power spectrum can nonetheless be useful as a time-averaged representation of how the system behaves, even if the real-world semivariogram or power spectrum is non-stationary. The situation is analogous to timing the velocity of a flock of birds. Even if each bird flies at a different (and time-varying) speed, and even if the average velocity of the flock varies through time, the time-averaged (and flock-averaged) velocity is still a measurable and useful aggregate representation of the birds' behaviour. This time-averaged and flock-averaged velocity obviously does not apply to every individual bird at every point in time. Likewise, the semivariograms and power spectra presented here are aggregate representations of the catchments' average behaviour, and do not apply at every point in time.

POWER SPECTRA

Fourier transform power spectra are often the analytical tool of choice for quantifying the intensity of fluctuations and their distribution across frequencies. Care must be taken to minimize several artifacts that can arise in spectral analysis of time series that are relatively short and irregularly sampled, like those from our two study catchments. Here, we used the date-compensated discrete Fourier transform (DCDFT, Ferraz-Mello, 1981; Foster, 1996) rather than the better-known Lomb-Scargle Fourier transform (Scargle, 1982), because of a potential artifact in the latter (Foster, 1995; Cumming *et al.*, 1999;

Shrager, 2001). We band-averaged the resulting power spectra using a Gaussian smoothing window with a characteristic width of 0·1 log units in frequency. We then used the alias-filtering technique of Kirchner (2005) to correct for the aliasing of spectral power from outside the measurable frequency range (that is, above the Nyquist frequency, here estimated as half of the median sampling frequency).

Figure 5 shows the resulting spectra. The vertical axes of both panels span the same number of log units; thus, the same vertical distance between the precipitation and streamflow spectra corresponds to the same fluctuation damping for either tracer at either site. For clarity, the axes have been adjusted to align the precipitation spectra for the two tracers, so that differences in fluctuation damping between the two tracers can be estimated from the relative levels of the streamflow spectra. Figure 5 shows that fluctuations in $\delta^{18}O$ are more strongly damped than those in Cl^-, that both tracers are more strongly damped at the Mharcaidh catchment than at the Girnock, and that these patterns persist almost without exception across the full range of frequencies present in the time series data, reflecting fluctuations on timescales of weeks to years.

Despite the tendency for ^{18}O to be more strongly damped than Cl^-, both tracers exhibit similar patterns of damping as a function of frequency. This indicates that the travel-time distributions for the two tracers have similar shapes, because the shape of a travel-time distribution is mathematically related to its corresponding pattern of frequency-dependent fluctuation damping via the Convolution Theorem. Thus, one can estimate the shape of the travel-time distribution from the damping of conservative tracers as a function of frequency. The relevant mathematics can be briefly summarized as follows.

The concentration time series of a conservative tracer in streamflow will be determined by the convolution of the time series in precipitation and the travel-time distribution:

$$c_S(t) = \int_0^\infty h(\tau) \quad c_R(t-\tau) \quad \mathrm{d}\tau \tag{3}$$

Equation (3) says that the concentration time series of a conservative tracer in streamflow $c_S(t)$ will be determined by the average of the concentrations in precipitation through all previous time $c_R(t-\tau)$, weighted by the travel-time distribution $h(\tau)$, where τ denotes the lag time between the input and the output. The travel-time distribution $h(\tau)$ expresses the fractional contribution of past inputs to the present runoff.

The convolution expressed in Equation (3) ignores the effects of evaporation on tracer concentrations. Furthermore, because the flow rate through the catchment varies through time, Equation (3) is strictly valid when t and τ are expressed in terms of the cumulative flow through the catchment rather than calendar time. However, most analyses of catchment travel-time distributions use Equation (3) as shown above, in units of calendar time; this is equivalent to assuming that the water fluxes

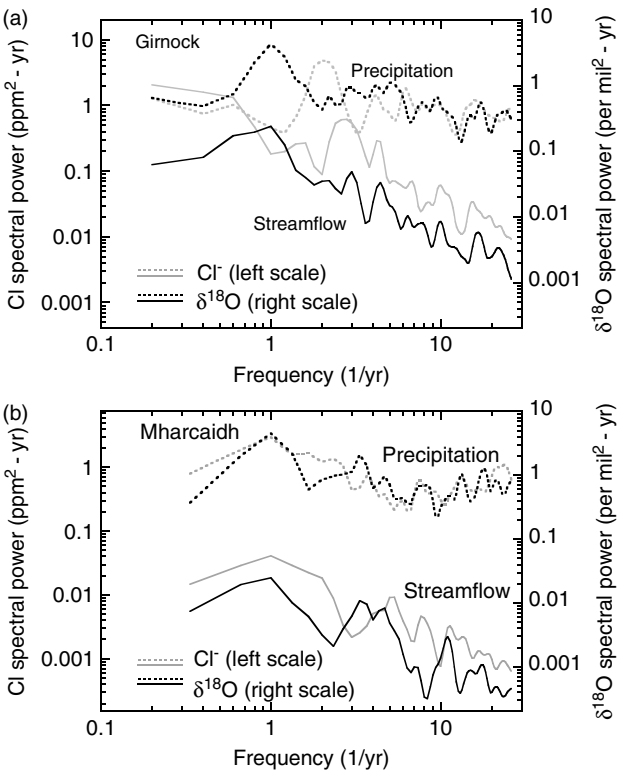

Figure 5. Power spectra of fluctuations in Cl^- and $\delta^{18}O$ (grey and black lines, respectively) in precipitation and streamflow (dashed and solid lines, respectively) at the Girnock and Mharcaidh catchments. Each vertical axis spans the same number of log units; thus, the same vertical distance between the precipitation and streamflow spectra implies the same fluctuation damping for either tracer at either site. For clarity, the axes have been adjusted to overlay the precipitation spectra for the two tracers, so that differences in fluctuation damping between the two tracers can be estimated from the relative levels of the streamflow spectra. At both sites, ^{18}O is somewhat more strongly damped than Cl^- across almost the full range of frequencies. Also, both tracers are more strongly damped at the Mharcaidh catchment than at the Girnock, across the full range of frequencies. However, both tracers exhibit similar patterns of damping as a function of frequency, indicating that their travel-time distributions have similar shapes

in precipitation and streamflow are constant, and only the concentrations vary through time. The result will only be an approximation to the real-world travel-time distribution, which will not be time-invariant, but instead will be stretched or compressed (as a function of lag time) as the water fluxes through the catchment vary.

The Convolution Theorem states that, for a system governed by a convolution integral such as (3) above, the Fourier transforms of the input time series, the output time series, and the travel-time distribution are connected by a simple multiplicative relationship:

$$C_S(f) = H(f) \quad C_R(f) \tag{4}$$

where $C_R(f)$ and $C_S(f)$ are the Fourier transforms of the precipitation and streamflow time series, respectively, and $H(f)$ is the Fourier transform of the travel-time distribution. Equation (4) in turn implies that the corresponding power spectra also obey a simple multiplicative relationship:

$$S_{C_S}(f) = S_H(f)\ S_{C_R}(f) \tag{5}$$

The power spectrum $S_H(f)$ of the travel-time distribution expresses how much fluctuations in the output are damped (or, at least theoretically, amplified) relative to the input. For this reason, $S_H(f)$ is termed the *transfer function*: it determines how much of the input power at any given frequency is transmitted to the output.

Comparing power spectra (as in Equation 5) discards any phase information contained in the Fourier transforms (as in Equation 4), and thus ignores any information contained in the relative timing of the precipitation and streamflow fluctuations. Therefore, Equation (5) will be unable to distinguish between different travel-time distributions that are otherwise identical except for a shift forward or backward in time (as in, for example, an exponential piston flow model). However, in practical applications to real-world precipitation and streamflow tracer time series, the relative phases of the Fourier transforms usually cannot be reliably determined. Thus, it is actually advantageous to discard the phase information, because the relationship between the fluctuation amplitudes (or the spectral powers) can be well constrained even if the phase relationships cannot. In the process one loses the ability to detect time-shifts of the travel-time distribution, but they would not have been detectable anyway, given the nature of the data at hand.

In principle, one should be able to infer the travel-time distribution directly from data by the method of *spectral deconvolution*, in which one first takes the Fourier transforms of the precipitation and streamflow tracer time series, then inverts Equation (4) to calculate $H(f)$ from $C_R(f)$ and $C_S(f)$, and then takes the inverse Fourier transform of $H(f)$ to recover $h(\tau)$. However, in practice the spectral deconvolution approach cannot be applied to catchment data because it is too sensitive to measurement noise and uneven sampling in the precipitation time series. Instead, one adopts a *forward spectral convolution* approach, in which one assumes a suitable form for the travel-time distribution $h(\tau)$, calculates its spectral power $S_H(f)$, and tests whether it satisfies Equation (5).

Here, we illustrate this approach, using the gamma distribution as our model for the catchments' travel-time distributions. We use the gamma distribution because it encompasses a wide range of shapes that could potentially describe catchment travel-time distributions, and because its power spectrum can be calculated straightforwardly. The gamma distribution is expressed mathematically as

$$h(\tau) = \frac{\tau^{\alpha-1}}{\beta^{\alpha}\,\Gamma(\alpha)} e^{-\tau/\beta} = \frac{\tau^{\alpha-1}}{(\tau_o/\alpha)^{\alpha}\,\Gamma(\alpha)} e^{-\alpha\tau/\tau_o} \qquad (6)$$

where the scale factor $\beta = \tau_o/\alpha$ re-scales the distribution and the shape factor α determines its shape. The gamma distribution is typically given in the β-form above, but we also show the τ_o-form to make the dependence on the mean travel time (τ_o) explicit.

Figure 6 shows examples of the gamma distribution for a range of shape factors. For the special case in which $\alpha = 1$, the gamma distribution becomes the exponential distribution, which expresses the response of a linear reservoir (often called a continuously stirred tank reactor in the engineering literature) of constant volume. For integer values of α, the gamma distribution yields the travel-time distribution expected for a so-called Nash cascade (Nash, 1957) of linear reservoirs connected in series. The distribution of travel times in a Nash cascade, also called an Erlang distribution, is a gamma distribution in which α is set to the number of reservoirs, and β is the mean travel time in each reservoir (or equivalently, τ_o is the mean travel time in the whole reservoir cascade). Yet another special case is the chi-squared distribution, which is a gamma distribution in which β equals two and the shape parameter α is the number of degrees of freedom divided by two.

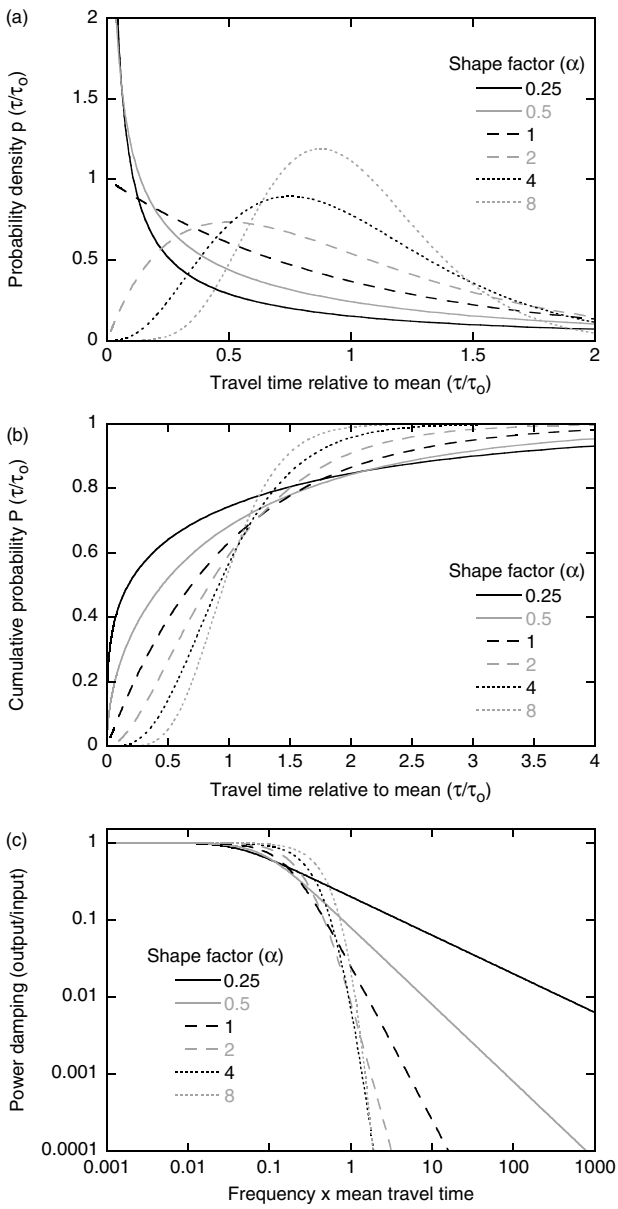

Figure 6. Probability density functions (a), cumulative distribution functions (b) and transfer functions (c) for gamma distributions with a range of shape factors α. When $\alpha < 1$, gamma distributions have substantial weight at travel times close to zero (panel a) and long upper tails (panel b). Gamma distributions with larger shape factors damp high-frequency fluctuations more strongly than those with smaller shape factors do (panel c)

For $\alpha > 1$, the gamma distribution rises to a peak and then falls off, similarly to a typical storm hydrograph; for this reason, the Nash cascade has often been used to model rainfall–runoff relationships. For $\alpha < 1$, however, the gamma distribution has a completely different shape, with maximum weight at lags near zero, and a relatively long tail (Figure 6). Both the large weight near zero and the long tail are reasons for concern in the case of contaminant transport; they imply that a pulse input of a contaminant would be transmitted through the catchment as both an intense spike of contamination in the near term, and a long tail of persistent pollution in the long term (Godsey *et al*., 2010).

Lower values of the shape factor α indicate greater variability in travel times relative to the mean. Mathematically one can express the standard deviation of the gamma distribution straightforwardly as:

$$\text{SD}\ (\tau) = \tau_o/\sqrt{\alpha} \tag{7}$$

For $\alpha = 1$ (the exponential distribution), the standard deviation of the travel-time distribution equals its mean. As α increases above 1, the standard deviation declines as the distribution becomes more peaked. But as α decreases below 1, the standard deviation grows hyperbolically, implying greater and greater variability in travel times, with more short and long travel times, and fewer close to the average.

The complex Fourier transform $H(f)$ of the gamma distribution (also termed its 'characteristic function' in probability theory) is:

$$H(f) = (1 - i\omega\ \beta)^{-\alpha} = (1 - 2\pi\ i\ f\ \tau_o/\alpha)^{-\alpha} \tag{8}$$

where $\omega = 2\pi f$ is the angular frequency in radians/time and, as before, the scale factor β is τ_o/α. Multiplying (8) by its complex conjugate gives the power spectrum of the travel-time distribution,

$$S_H(f) \equiv H(f)\ H^*(f) = \left(1 + (2\pi\ f\ \tau_o/\alpha)^2\right)^{-\alpha} \tag{9}$$

One can see that at frequencies that are low in relation to the reciprocal of the mean travel time (such that $2\pi f \tau_o/\alpha << 1$), the transfer function will be close to 1 and fluctuations in the input will be transmitted to the output with little attenuation. Conversely, at frequencies that are high in relation to the reciprocal of the mean travel time (such that $2\pi f \tau_o/\alpha >> 1$), the transfer function will be much less than 1 and fluctuations in the input will be strongly attenuated with increasing frequency, falling off as a power function of frequency that becomes steeper with increasing α, with $S_H(f) \sim 1/f^{2\alpha}$.

Combining Equations (9) and (5), one obtains the following relationship between the spectral power of tracer fluctuations in precipitation and streamflow:

$$\hat{S}_{C_S}(f) = \left(1 + (2\pi\ f\ \tau_o/\alpha)^2\right)^{-\alpha}\ S_{C_R}(f) \tag{10}$$

where $\hat{S}_{C_S}(f)$ is the estimated spectrum of the tracer concentrations in streamflow, estimated from the spectra of the rainfall concentrations and the travel-time distribution. One can then estimate the shape factor α and mean travel time τ_o by adjusting their values in Equation (10) until the predicted spectral power in streamflow $\hat{S}_{C_S}(f)$ agrees with the measured spectrum $S_{C_S}(f)$ as closely as possible (as measured by the root-mean-square deviation between the logarithms of the modelled and measured spectra).

Table III and Figures 7 and 8 show the results of this approach for Cl^- and ^{18}O at the two study catchments. Figure 7 shows that the modelled stream tracer spectra are generally similar to the measured spectra, although they differ in detail. As quantified in Table III, the best-fit values of the shape factor α vary somewhat between the two tracers and between the two sites, ranging from 0·35 to 0·59. However, these α values are not statistically distinguishable, because in every case they lie within two standard errors of one another. The best-fit values of the mean travel time τ_o vary widely, from 0·15 to 11 years, and in most cases the standard errors of the τ_o estimates are similar to, or even larger than, the estimates themselves. In each case the τ_o values are statistically undistinguishable from one another.

These large uncertainties arise because the two parameters, α and τ_o, have largely offsetting effects on the modelled spectra, with the result that the correlation between the α and τ_o estimates exceeds −0·94 in every case, and even reaches −0·99 in two cases (Table III). As Figure 8a shows, the best-fit estimate of the mean travel time τ_o is highly sensitive to the corresponding value of the shape factor α, particularly when α is well below 1, as is the

Table III. Gamma travel-time distributions estimated from tracer fluctuation power spectra

Site	Tracer	Record length	Shape factor α	Mean travel time τ_o (yr)	Parameter correlation (α, τ_o)	Mean travel time, α fixed at 0·5 (yr)
Girnock:						
	$\delta^{18}O$	5 yr	0·35 ± 0·06	2·60 ± 2·16	−0·98	0·61 ± 0·10
	Cl^-	5 yr	0·55 ± 0·14	0·15 ± 0·08	−0·94	0·18 ± 0·03
Mharcaidh:						
	$\delta^{18}O$	3 yr	0·43 ± 0·16	11·31 ± 27·31	−0·99	4·87 ± 1·47
	Cl^-	3 yr	0·44 ± 0·18	4·09 ± 8·89	−0·99	2·28 ± 0·74
	Cl^-	16 yr	0·59 ± 0·13	0·61 ± 0·42	−0·97	1·10 ± 0·25

Uncertainties are expressed as ±1 standard error. Standard errors have been re-scaled to account for loss of degrees of freedom due to correlation in residuals.

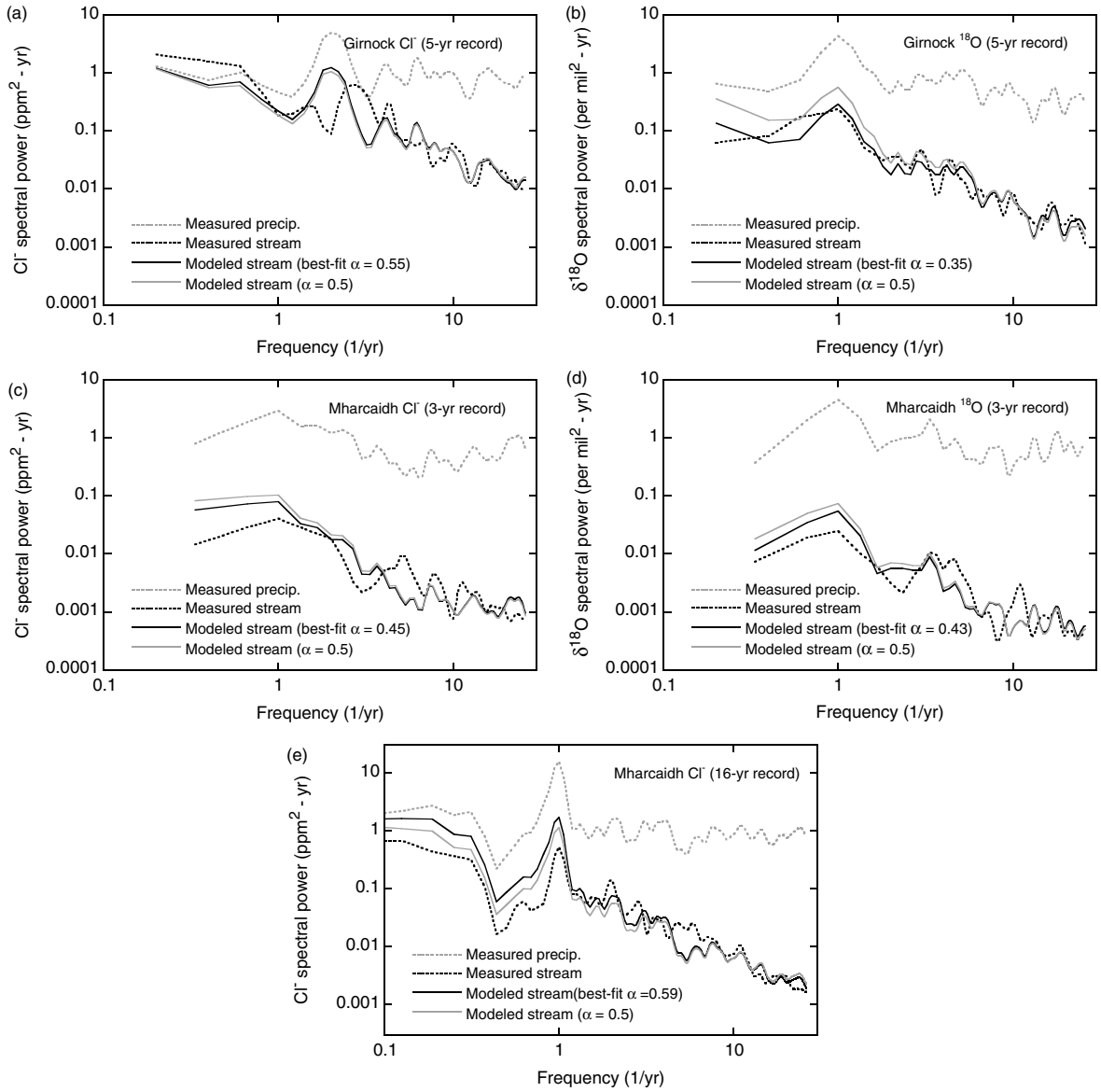

Figure 7. Power spectra of tracer concentrations in precipitation and streamflow at the Girnock and Mharcaidh catchments (dotted lines), compared to streamflow tracer spectra modelled using gamma travel-time distributions (solid lines). Two modelled spectra are shown: one for the best-fit value of the shape factor α, which varies among the plots (black solid lines), and another for a fixed α of 0·5 (grey solid lines)

case for the tracer data analysed here. As a result, it will be difficult to distinguish between the spectral effects of a travel-time distribution with a relatively small α but a relatively large τ_o, and a distribution with a larger α but a smaller τ_o. As Figure 8b shows, the goodness of fit of the modelled and measured spectra varies only gradually as α changes and τ_o shifts to compensate, with the result that α (and thus τ_o) are not tightly constrained by the available data. This problem is particularly acute when the tracer time series are relatively short and infrequently sampled, and thus their spectra span relatively limited frequency ranges. This is the case at these study sites, where we have only a few years of weekly sampled data (rather than, for example, decades of weekly samples or years of daily samples). When the mean travel time is similar to, or even greater than, the length of the available time series, the estimates of both α and τ_o will be poorly constrained. Nonetheless, the curves relating τ_o to α for our study sites are well defined (Figure 8a); it is just difficult to determine which point along each curve describes each catchment.

If one knows or assumes the value of the shape factor α in advance, however, the mean travel time is much more strongly constrained by the measured spectra. The last column of Table III shows the best-fit mean travel times for an assumed shape factor of $\alpha = 0{\cdot}5$, which has been chosen because it is broadly consistent with the shape factors that have been estimated for these sites and many others (e.g. Kirchner *et al.*, 2000, 2001; Godsey *et al.*, 2010). Under this assumption, as the last column of Table III shows, the mean travel time is much better constrained, with standard errors of 20%–30%, compared to the much larger standard errors when α is treated as a fitting parameter. The estimated mean travel times are consistently longer at the Mharcaidh catchment than the Girnock (by a factor of approximately 6–10), and

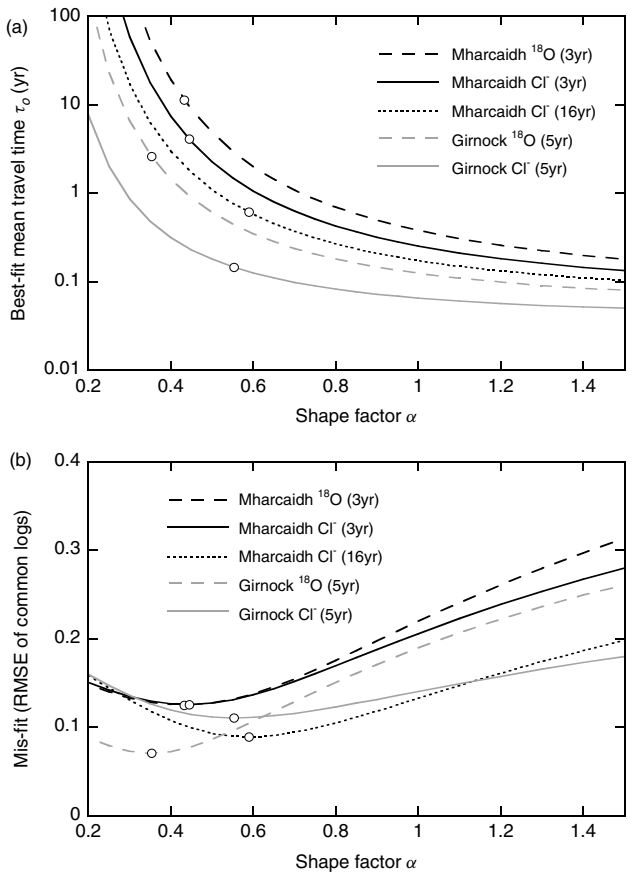

Figure 8. (a) Dependence of best-fit mean travel time τ_o on the shape factor α for each of the spectra shown in Figure 7, estimated by fixing the value of α and finding the corresponding value of τ_o that minimizes the sum of squared deviations between the predicted and observed logarithms of the stream tracer spectrum. (b) Variation in mis-fit between predicted and observed stream tracer spectra, quantified as the root-mean-squared error in logs, as a function of the shape factor α. Circles indicate global best-fit parameter values for each spectrum

consistently longer for ^{18}O than for Cl^- (by a factor of approximately 2 or 3), consistent with the differences in variance damping observed between the sites and between the tracers. The modelled stream tracer spectra for $\alpha = 0{\cdot}5$ and the best-fit value of τ_o, shown Figure 7 as solid grey lines, are virtually indistinguishable from those for which both α and τ_o have been optimized, shown in Figure 7 as solid black lines.

DISCUSSION

Three lines of evidence indicate that ^{18}O and Cl^- behave similarly as tracers of transport, storage and mixing at our two study sites. (1) Both tracers are strongly damped in streamflow, relative to precipitation, at both sites, as shown in Table II and Figures 2 and 3. (2) The pattern of damping of variance as a function of lag time is similar for both tracers, as shown by the semivariograms in Figure 4. (3) Both tracers' power spectra show similar patterns of fluctuation damping as a function of frequency (Figure 5), implying that the travel-time distributions of both tracers have similar shapes (Figure 7; Table III).

Both ^{18}O and Cl^- are more strongly damped, relative to precipitation inputs, at the Mharcaidh catchment than at the Girnock. This may seem counterintuitive because the Mharcaidh catchment is both smaller and steeper overall (Table I), and McGuire *et al*. (2005) have reported shorter mean travel times associated with steeper hillslope gradients at the H.J. Andrews Experimental Forest. In Scottish catchments like ours, however, travel times may be determined less by topography, and more by variations in the hydrological behaviour of soils (Soulsby *et al*., 2004; Soulsby *et al*., 2006; Tetzlaff *et al*., 2009). Hydraulically responsive soils such as peats and gleys are more closely connected to the stream channel in the Girnock catchment than in the Mharcaidh. Steeper slopes, which are more common in the Mharcaidh catchment, are also more likely to have freely draining soils, thereby contributing to groundwater recharge and to longer travel times (Soulsby *et al*., 2006).

Quantitative estimates of mean travel times are sensitive to the assumed shape of the travel-time distribution (which, for the gamma distributions considered here, is expressed by the shape factor α). As Figure 8 and Table III show, estimates of mean travel time are strongly and negatively correlated with the shape factor α. This problem of parameter identifiability is not specific to the spectral analysis techniques used in Figure 7; it arises in time-domain convolution analyses as well (McGuire and McDonnell, 2006). Most estimates of travel times are based on an assumed exponential distribution ($\alpha = 1$), or a dispersion model which rises to a peak and then falls again, similar to the gamma distribution for $\alpha > 1$ (McGuire and McDonnell, 2006, Table I). By contrast, where the shape of the travel-time distribution has been estimated from data, it has often been found to be significantly different from these assumed distributions, for example: $\alpha \approx 0{\cdot}5$ at the Plynlimon catchments (Kirchner *et al*., 2000), $0{\cdot}35 < \alpha < 0{\cdot}78$ in a survey of 20 catchments by Godsey *et al*. (2010), and $0{\cdot}35 < \alpha < 0{\cdot}59$ at the Girnock and Mharcaidh catchments (this study). The discrepancy between the assumed and observed shapes of travel-time distributions is important because, as Figure 8a makes clear, overestimates of α will be associated with underestimates of the mean travel time. Thus, analyses that assume $\alpha = 1$ or $\alpha > 1$ will underestimate the mean travel time, potentially by large factors, wherever the true travel-time distribution is characterized by $\alpha < 1$. This observation highlights the need to determine the shapes of travel-time distributions for many diverse catchments. The major limitation to such efforts will be the scarcity of tracer time series that are sampled frequently enough, and for long enough, to permit the shape of the travel-time distribution to be reliably estimated.

The three lines of evidence outlined above—variances, semivariograms and power spectra—all suggest that ^{18}O is more strongly damped than Cl^- at both the Mharcaidh and Girnock catchments (Table II; Figures 4 and 5). The stronger damping of ^{18}O relative to Cl^- leads to longer estimated mean travel times, by factors of two to three, for ^{18}O compared to Cl^- (Table III). However, it is

physically implausible that Cl^- would move through a catchment at two or three times the speed of the water that carries it. Instead, it seems plausible that the greater variability of Cl^- concentrations arises from spatially and temporally variable evaporation and evapotranspiration (which will proportionally alter concentrations of solutes like Cl^-, but will only incrementally fractionate ^{18}O), and from dry and occult deposition of Cl^-. Similar considerations were invoked by Neal and Rosier (1990) to explain the greater damping in ^{18}O compared to Cl^- at Plynlimon in mid-Wales. If catchments generally exhibit greater damping of ^{18}O than Cl^-, as observed at Plynlimon and our Scottish sites, then estimates of mean travel times derived from Cl^- fluctuations will usually be shorter than those derived from ^{18}O fluctuations. This possibility should be kept in mind when comparing mean travel time estimates obtained from different tracers at different sites.

Nonetheless, it is the similarities, not the differences, in the behaviour of ^{18}O and Cl^- that are most striking. The variance of ^{18}O is damped more than the variance of Cl^-, by a factor of 0·9–3·6 (median 1·6) across all the comparisons in Table II. However, this is only a small fraction of the total damping of the variance of ^{18}O in streamflow relative to precipitation, which ranges from a factor of 8 to a factor of 134 (median 32) across the same comparisons. The common damping behaviour that the two tracers share, across a wide range of time scales (Figure 4) and fluctuation frequencies (Figure 5), is much more pronounced than the relatively small differences between them.

One cannot attribute the strong damping in ^{18}O and Cl^- to artifacts, such as evapoconcentration and dry or occult deposition (in the case of Cl^-) or evaporative fractionation (in the case of ^{18}O). It is implausible that these different artifacts would produce nearly the same degree of damping in both tracers. And in any case, to the extent that these artifacts are spatially and temporally variable, they would increase the variances of tracer concentrations in streamflow and thus would reduce the apparent degree of tracer damping in the catchment. Likewise, it is implausible that it is just by chance that these two tracers, whose fluctuations in precipitation are uncorrelated with one another, are damped by nearly the same amounts, across a wide range of time scales and fluctuation frequencies (Figures 4 and 5). Instead, the only plausible explanation for the similarities in the damping behaviour of the two tracers is that they both 'follow the water', and that therefore they are both are stored and mixed (and thus their fluctuations are damped) in similar ways.

The strong damping of fluctuations in both ^{18}O and Cl^- implies that runoff at both the Girnock and Mharcaidh catchments is primarily composed of pre-event water. Equivalently, it implies that these catchments store and mix volumes of water that are much larger than individual storms, on timescales that are much longer than the intervals between events. Nonetheless, both catchments respond rapidly to precipitation, with streamflows rising by orders of magnitude within hours following the onset of rainfall. How do these catchments (and the many other catchments that behave similarly) store water for months or years, but then mobilize it within hours in response to rainfall inputs? Finding mechanisms behind this paradoxical behaviour remains a major challenge for catchment hydrologists. Reliable tracers of storage and mixing are important tools both for documenting this paradox and for working to resolve it.

ACKNOWLEDGEMENTS

Many individuals have contributed to the datasets for the two catchments, including Iain Malcolm and Phil Bacon (Freshwater Lab, Marine Scotland), Susan Waldron (University of Glasgow), Paul Rodgers and Mark Speed (University of Aberdeen), Bob Ferrier (Macaulay Institute) and Jo and Molly Porter. Similarly, many agencies funded the data collection and sample analysis, including The Scottish Government, the Leverhulme Trust, NERC and DEFRA. We thank Sarah Godsey for helpful discussions. Our analysis was partly supported by NSF grant EAR-0125550 to JWK, and by the Berkeley Water Center. Early phases of this analysis were conducted while JWK was supported by the Miller Institute for Basic Research.

REFERENCES

Bastviken D, Sanden P, Svensson T, Stahlberg C, Magounakis M, Oberg G. 2006. Chloride retention and release in a boreal forest soil: effects of soil water residence time and nitrogen and chloride loads. *Environmental Science and Technology* **40**: 2977–2982.

Bastviken D, Thomsen F, Svensson T, Karlsson S, Sanden P, Shaw G, Matucha M, Oberg G. 2007. Chloride retention in forest soil by microbial uptake and by natural chlorination of organic matter. *Geochimica Et Cosmochimica Acta* **71**: 3182–3192.

Bracewell RN. 2000. *The Fourier Transform and its Applications* (3rd ed.). McGraw Hill: Boston.

Buttle JM. 1994. Isotope hydrograph separations and rapid delivery of pre-event water from drainage basins. *Progress in Physical Geography* **18**: 16–41.

Cumming A, Marcy GW, Butler RP. 1999. The Lick planet search: Detectability and mass thresholds. *The Astrophysical Journal* **526**: 890–915.

Dunn SM, Bacon JR. 2008. Assessing the value of Cl2 and $\delta^{18}O$ data in modelling the hydrological behaviour of a small upland catchment in northeast Scotland. *Hydrology Research* **39**: 337–358.

Fenicia F, McDonnell JJ, Savenije HHG. 2008. Learning from model improvement: On the contribution of complementary data to process understanding. *Water Resources Research* **44**: W06419.

Ferraz-Mello S. 1981. Estimation of periods from unequally spaced observations. *Astronomical Journal* **86**: 619–624.

Foster G. 1995. The CLEANEST Fourier spectrum. *Astronomical Journal* **109**: 1889–1902.

Foster G. 1996. Time series analysis by projection. 1. Statistical properties of Fourier analysis. *Astronomical Journal* **111**: 541–554.

Gelhar LW. 1993. *Stochastic Subsurface Hydrology*. Prentice-Hall: Englewood Cliffs, N.J.

Godsey SE, Aas W, Clair TA, de Wit HA, Fernandez IJ, Kahl JS, Malcolm IA, Neal C, Neal M, Nelson SJ, Norton SA, Palucis MC, Skjelkvåle BL, Soulsby C, Tetzlaff D, Kirchner JW. 2010. Generality of fractal 1/f scaling in catchment tracer time series, and its implications for catchment travel time distributions. *Hydrological Processes* **24**: 1660–1671.

Grimaldi C, Thomas Z, Fossey M, Fauvel Y, Merot P. 2009. High chloride concentrations in the soil and groundwater under an oak hedge in the West of France: an indicator of evapotranspiration and water movement. *Hydrological Processes* **23**: 1865–1873.

Hooper RP, Shoemaker CA. 1986. A comparison of chemical and isotopic hydrograph separation. *Water Resources Research* **22**: 1444–1454.

Hrachowitz M, Soulsby C, Tetzlaff D, Dawson JJC, Malcolm IA. 2009. Regionalization of transit time estimates in montane catchments by integrating landscape controls. *Water Resources Research* **45**: W05421. DOI:05410.01029/02008WR007496.

Jenkins A, Ferrier RC, Harriman R, Ogunkoya YO. 1994. A case-study in catchment hydrochemistry—conflicting interpretations from hydrological and chemical observations. *Hydrological Processes* **8**: 335–349.

Jobbagy EG, Jackson RB. 2007. Groundwater and soil chemical changes under phreatophytic tree plantations. *Journal of Geophysical Research-Biogeosciences* **112**: G02013. DOI:02010.01029/02006JG000246.

Kendall C, and Caldwell EA. 1998. Fundamentals of isotope geochemistry. In *Isotope Tracers in Catchment Hydrology*, Kendall C, McDonnell JJ (eds). Elsevier: Amsterdam; 51–86.

Kirchner JW, Feng X, Neal C. 2000. Fractal stream chemistry and its implications for contaminant transport in catchments. *Nature* **403**: 524–527.

Kirchner JW, Feng X, Neal C. 2001. Catchment-scale advection and dispersion as a mechanism for fractal scaling in stream tracer concentrations. *Journal of Hydrology* **254**: 81–100.

Kirchner JW. 2005. Aliasing in $1/f^{\alpha}$ noise spectra: Origins, consequences, and remedies. *Physical Review E (Statistical, Nonlinear, and Soft Matter Physics)* **71**: 066110.

Martinec J, Siegenthaler U, Oeschger H, and Tongiorgi E. 1974. New insights into the run-off mechanism by environmental isotopes. In *Isotope Techniques in Groundwater Hydrology* IAEA: Vienna; 129–149.

McDonnell JJ, Bonell M, Stewart MK, Pearce AJ. 1990. Deuterium variations in storm rainfall—Implications for stream hydrograph separation. *Water Resources Research* **26**: 455–458.

McGuire KJ, McDonnell JJ, Weiler M, Kendall C, McGlynn BL, Welker JM, Seibert J. 2005. The role of topography on catchment-scale water residence time. *Water Resources Research* **41**: W05002.

McGuire KJ, McDonnell JJ. 2006. A review and evaluation of catchment transit time modeling. *Journal of Hydrology* **330**: 543–563.

Nash JE. 1957. The form of the instantaneous unit hydrograph. *Comptes Rendus et Rapports, IASH General Assembly Toronto 1957. International Association of Scientific Hydrology (Gentbrugge)* **3**: 114–121.

Neal C, Christophersen N, Neale R, Smith CJ, Whitehead PG, Reynolds B. 1988. Chloride in precipitation and streamwater for the upland catchment of the River Severn, mid-Wales: some consequences for hydrochemical models. *Hydrological Processes* **2**: 155–165.

Neal C, Rosier PTW. 1990. Chemical studies of chloride and stable oxygen isotopes in 2 conifer afforested and moorland sites in the British uplands. *Journal of Hydrology* **115**: 269–283.

Neal C, Neal M, Warrington A, Avila A, Pinol J, Roda F. 1992. Stable hydrogen and oxygen isotope studies of rainfall and streamwaters for two contrasting holm oak areas of Catalonia, northeastern Spain. *Journal of Hydrology* **140**: 163–178.

Page T, Beven KJ, Freer J, Neal C. 2007. Modelling the chloride signal at Plynlimon, Wales, using a modified dynamic TOPMODEL incorporating conservative chemical mixing (with uncertainty). *Hydrological Processes* **21**: 292–307.

Pearce AJ, Stewart MK, Sklash MG. 1986. Storm runoff generation in humid headwater catchments. 1. Where does the water come from. *Water Resources Research* **22**: 1263–1272.

Robins NS. 1990. *Hydrogeology of Scotland*. H.M.S.O.: London.

Scargle JD. 1982. Studies in astronomical time series analysis. II. Statistical aspects of spectral analysis of unevenly spaced data. *The Astrophysical Journal* **263**: 835–853.

Shrager RI. 2001. On a three-term variant of the Lomb periodogram. *Astrophysics and Space Sciences* **277**: 519–530.

Sklash MG, Farvolden RN. 1979. The role of groundwater in storm runoff. *Journal of Hydrology* **43**: 45–65.

Soulsby C, Helliwell RC, Ferrier RC, Jenkins A, Harriman R. 1997. Seasonal snowpack influence on the hydrology of a sub-arctic catchment in Scotland. *Journal of Hydrology* **192**: 17–32.

Soulsby C, Chen M, Ferrier RC, Helliwell RC, Jenkins A, Harriman R. 1998. Hydrogeochemistry of shallow groundwater in an upland Scottish catchment. *Hydrological Processes* **12**: 1111–1127.

Soulsby C, Malcolm R, Helliwell R, Ferrier RC, Jenkins A. 2000. Isotope hydrology of the Allt a' Mharcaidh catchment, Cairngorms, Scotland: implications for hydrological pathways and residence times. *Hydrological Processes* **14**: 747–762.

Soulsby C, Rodgers PJ, Petry J, Hannah DM, Malcolm IA, Dunn SM. 2004. Using tracers to upscale flow path understanding in mesoscale mountainous catchments: two examples from Scotland. *Journal of Hydrology* **291**: 174–196.

Soulsby C, Malcolm IA, Youngson AF, Tetzlaff D, Gibbins CN, Hannah DM. 2005. Groundwater-surface water interactions in upland Scottish rivers: hydrological, hydrochemical, and ecological implications. *Scottish Journal of Geology* **41**: 39–49.

Soulsby C, Tetzlaff D, Rodgers P, Dunn S, Waldron A. 2006. Runoff processes, stream water residence times and controlling landscape characteristics in a mesoscale catchment: an initial evaluation. *Journal of Hydrology* **325**: 197–221.

Soulsby C, Tetzlaff D, van den Bedem N, Malcolm IA, Bacon JR, Youngson AF. 2007. Inferring groundwater influences on surface water in montane catchments from hydrochemical surveys of springs and streamwaters. *Journal of Hydrology* **333**: 199–213.

Tetzlaff D, Malcolm IA, Soulsby C. 2007a. Influence of forestry, environmental change and climatic variability on the hydrology, hydrochemistry and residence times of upland catchments. *Journal of Hydrology* **346**: 93–111.

Tetzlaff D, Soulsby C, Waldron A, Malcolm IA, Bacon JR, Dunn SM, Lilly A, Youngson AF. 2007b. Conceptualization of runoff processes using a geographical information system and tracers in a nested mesoscale catchment. *Hydrological Processes* **21**: 1289–1307.

Tetzlaff D, Seibert J, McGuire KJ, Laudon H, Burns DA, Dunn S, Soulsby C. 2009. How does landscape structure influence catchment transit time across different geomorphic provinces?. *Hydrological Processes* **23**: 945–953.

Webster R, Oliver MA. 2007. *Geostatistics for Environmental Scientists* (2nd edition). Wiley: New York.

Wheater HS, Tuck S, Ferrier RC, Jenkins A, Kleissen FM, Walker TAB, Beck MB. 1993. Hydrological flow paths at the Allt a Mharcaidh catchment—an analysis of plot and catchment scale observations. *Hydrological Processes* **7**: 359–371.

